arXiv:1403.6321v1 [nucl-th] 25 Mar 2014

Evolution of transverse flow and effective temperatures in the parton phase from a multi-phase transport model

Zi-Wei Lin

Department of Physics, East Carolina University,

C-209 Howell Science Complex, Greenville, NC 27858

Abstract

We study the space-time evolution of transverse flow and effective temperatures in the dense parton phase with the string melting version of a multi-phase transport model. Parameters of the model are first constrained to reproduce the bulk data on the rapidity density, $p_{\rm T}$ spectrum and elliptic flow at low $p_{\rm T}$ for central and mid-central Au+Au collisions at 200 AGeV and Pb+Pb collisions at 2760 AGeV. We then calculate the transverse flow and effective temperatures in volume cells within mid-spacetime-rapidity $|\eta| < 1/2$. We find that the effective temperatures extracted from different variables, which are all evaluated in the rest frame of a volume cell, can be very different. In particular, the effective temperatures extracted from the parton energy density or number density are often quite different than those extracted from the parton mean $p_{\rm T}$ or mean energy. For these collisions in general, effective temperatures extracted from the parton energy density or number density are higher than those extracted from the parton mean $p_{\rm T}$ in the inner part of the overlap volume, while the opposite occurs in the outer part of the overlap volume. We argue that this indicates that the dense parton matter in the inner part of the overlap volume is over-populated; we also find that all cells with energy density above 1 GeV/fm^3 are over-populated after a couple of fm/c.

PACS numbers: 12.38.Mh, 25.75.Ld, 25.75.Nq

I. INTRODUCTION

A dense matter consisting of partonic degrees of freedom, often called the quark-gluon plasma (QGP), has been created in ultra-relativistic heavy ion collisions at the Relativistic Heavy Ion Collider (RHIC) and the Large Hadron Collider (LHC). Its properties such as the color glass condensate initial condition, the degree of equilibration, event-by-event fluctuations, and coupling with high-momentum partons are being extensively studied [1–4]. Simulations of these collisions with hydrodynamic codes [5–8], transport models [9–11], or hybrid models [12–14] are able to produce the full evolution history of dense matter and are very useful for the studies of the quark-gluon plasma properties. In this paper we investigate the evolution of the parton matter at mid-spacetime-rapidity, including its transverse flow and effective temperatures. The string melting version of the AMPT model [10] is used here, where excited hadronic strings in the overlap volume are converted into partons via the intermediate step of decomposing hadrons that would have been produced by the Lund string fragmentation process [10, 15].

The default version of the AMPT model [16, 17] was first constructed to simulate relativistic heavy ion collisions, and its key parameters were determined to fit the yields and $p_{\rm T}$ spectra of particles in pp collisions at various energies and heavy ion collisions up to SPS energies. Hadronization in the default AMPT model is described by the Lund string model [18], where one assumes that a string fragments into quark-antiquark pairs with a Gaussian distribution in transverse momentum. Hadrons are formed from these quarks and antiquarks, with its longitudinal momentum given by the Lund symmetric fragmentation function $f(z) \propto z^{-1}(1-z)^a \exp(-b\ m_{\rm T}^2/z)$, where z represents the light-cone momentum fraction of the produced hadron with respect to that of the fragmenting string and $m_{\rm T}$ is the transverse mass of the hadron. We found [16, 17] that the default HIJING values for the Lund string fragmentation parameters ($a = 0.5$ and $b = 0.9$ GeV^{-2}), which work well for pp collisions, led to too small a charged particle yield in central Pb+Pb collisions at the SPS energy of $E_{\rm LAB}$ =158 AGeV. Therefore modified values of $a = 2.2$ and $b = 0.5$ GeV^{-2} were used in order to fit the charged particle yield in Pb+Pb collisions at SPS. For heavy ion collisions at higher

energies such as RHIC energies, the default version of the AMPT model with these parameters values was found to reasonably fit dN/dη, dN/dy and the $p_{\rm T}$ spectra in heavy ion collisions, although it under-estimates the elliptic flow. On the other hand, the string melting version of the AMPT model (AMPT-SM) [10, 15], due to its dense parton phase, reasonably fits the elliptic flow and two-pion HBT in heavy ion collisions; but it does not reproduce well dN/dη, dN/dy and the $p_{\rm T}$ spectra (when using the same parameters as in the default version). In particular, the AMPT-SM model significantly over-estimates the charged particle yield while under-estimates the slopes of the $p_{\rm T}$ spectra [10]. In an earlier attempt to reproduce data in Pb+Pb collisions at LHC energies with the AMPT-SM model, the default HIJING values for the Lund string fragmentation parameters were used [19] together with the strong coupling constant $\alpha_s = 0.33$ (instead of 0.47); there the model reasonably reproduced the yield and elliptic flow of charged particles but underestimated the $p_{\rm T}$ spectrum (except at low $p_{\rm T}$).

In this study we use the AMPT-SM model to study the evolution of the dense parton phase. We first tune the key parameters of the model to reproduce the pion and kaon yield, the pion and kaon $p_{\rm T}$ spectra, and the pion elliptic flow at low $p_{\rm T}$ (below ~ 2 GeV/c) in central and mid-central Au+Au collisions at the RHIC energy of 200 AGeV and Pb+Pb collisions at the LHC energy of 2760 AGeV. We then study the evolution of transverse flow and effective temperature in the parton phase. In our analysis, the reaction volume within $|\eta| < 1/2$ is divided into stationary cells with a transverse width of 1 fm. In order to have enough statistics for the analysis of each volume cell, we choose to study event-averaged quantities and thus neglect event-by-event fluctuations in this study. For each collision energy and centrality, we run hundreds to thousands of events at the same impact parameter range and then calculate event-averaged quantities at functions of time and transverse location. Note that the AMPT-SM model assigns a formation time to each parton produced from string melting [10], and only partons that have formed by a global time t are included in the analysis for that time. The full space-time evolution of the parton matter from this study will be posted online [20] and may be used as the bulk matter background within which other probes such as jet propagation and interactions can be studied [21, 22].

II. FITTING THE BULK DATA WITH THE STRING MELTING VERSION OF AMPT

In order to reasonably fit the low $p_{\rm T}$ data in central and mid-central Au+Au collisions at the top RHIC energy, we have changed the values of the Lund string fragmentation parameters to $a = 0.55$, $b = 0.15$ GeV^{-2}. When the Lund string fragmentation parameters are modified, the effective string tension, as given by $\kappa \propto 1/[b(2+a)]$ [10], will change. This will affect the mean transverse momentum of hadrons; in addition, the AMPT model assumes that the relative production of strange to non-strange quarks increases with the effective string tension [10]. Since the above string tension relation diverges as $b \to 0$ and this study uses a small b value to enable the AMPT-SM results to fit the data, we put an upper limit of 0.40 on the relative production of strange to non-strange quarks in AMPT. For Pb+Pb collisions at the LHC energy, we used $a = 0.30$ to in order to fit the ALICE data [23]. Note that the a value of 0.55 in the Lund model used for fitting the RHIC data gives a reasonable but less satisfactory fit of the ALICE data than the a value of 0.30. We take $\alpha_s = 0.33$ and a parton cross section of 3 mb for all simulations here.

AMPT-SM results shown in this study include four collision systems: RHIC central refers to Au+Au events at 200 AGeV with $b < 3$ fm that represent the 0-5% centrality, RHIC mid-central refers to Au+Au events at 200 AGeV with $b = 7.3$ fm that represent the 20-30% centrality [24], LHC central refers to Pb+Pb events at 2760 AGeV with $b < 3.5$ fm that represent the 0-5% centrality, and LHC mid-central refers to Pb+Pb events at 2760 AGeV with $b = 7.8$ fm that represent the 20-30% centrality [25]. Since each volume cell within $|\eta| < 1/2$ has a transverse width of 1.0 fm along both the x- and y-axis, the cell at $x = 3$ fm & $y = 0$ fm then refers to the volume within $2.5 < x < 3.5$ fm & $-0.5 < y < 0.5$ fm & $|\eta| < 1/2$, for example.

The comparisons between AMPT-SM results and the experimental data on particle dN/dy are shown in Fig. 1a for π^+ and in Fig. 1b for K^+, where we see reasonable agreements between the model results and the PHENIX [26] and ALICE data [23] at mid-rapidity in both central and mid-central events at RHIC and LHC energies. The comparisons of the π^+ and K^+ $p_{\rm T}$ spectra at mid-rapidity are shown in Fig. 2a

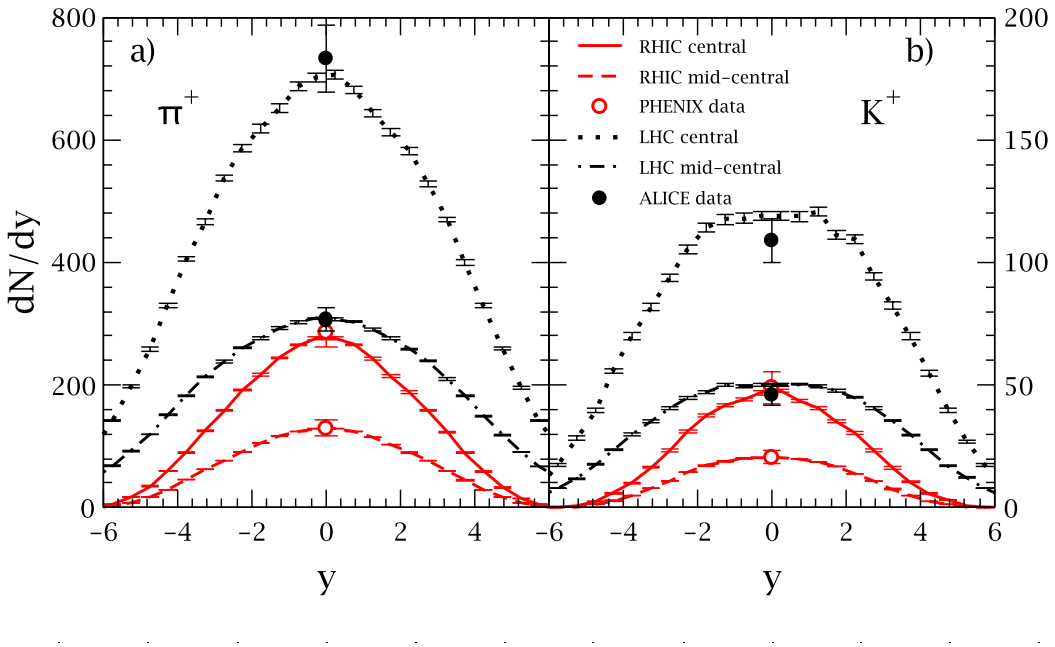

FIG. 1: AMPT-SM results for central and mid-central Au+Au collisions at $\sqrt{s_{NN}} = 200$ GeV and Pb+Pb collisions at $\sqrt{s_{NN}} = 2760$ GeV in comparison with experimental data for 0-5% and 20-30% centralities: a) dN/dy of π^+, and b) dN/dy of K^+.

and Fig. 2b respectively for central Au+Au collisions at the RHIC energy and central Pb+Pb collisions at the LHC energy, where the model roughly reproduces the observed $p_{\rm T}$ spectra below 2 GeV/c.

Fig. 3 shows the comparisons of $v_2\{\rm EP\}$ of charged pions. We see that the AMPT-SM model is also able to roughly reproduce the pion and kaon elliptic flow data on $v_2\{\rm EP\}$ [27] at low-$p_{\rm T}$. Note that the correction factor for the event plane resolution ${\rm Res}\{2\Phi_2\}$ [28] in the AMPT-SM results is calculated using particles within $-2.8 < y < -1$ and within $1 < y < 2.8$.

III. SPACE-TIME EVOLUTION OF TRANSVERSE FLOW

For each volume cell within $|\eta| < 1/2$, we calculate the flow as $\vec{\beta} = (\sum_i \vec{p}_i) \,/\, (\sum_i E_i)$, where the sum over index i takes into account all formed partons in the cell from all events of a given collision system. Fig. 4 shows the time evolutions of the transverse flow

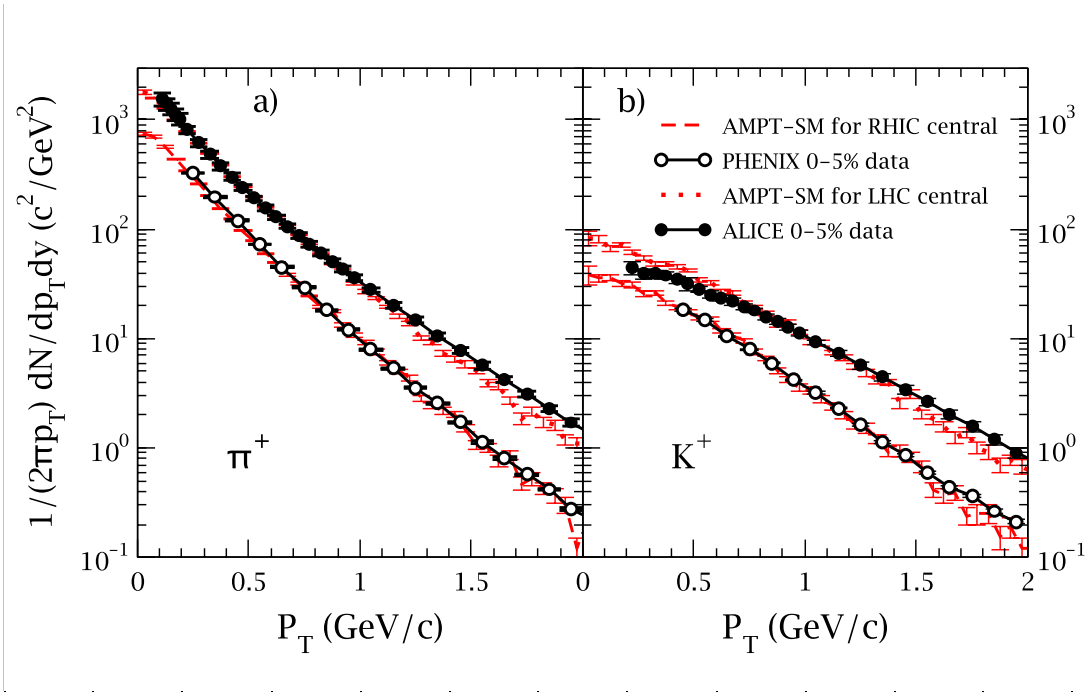

FIG. 2: $p_{\rm T}$ spectra of π^+ and K^+ at mid-rapidity in central collisions from AMPT-SM in comparison with experimental data for 0-5% centrality.

of partons in two cells in central Au+Au collisions at 200 AGeV: one cell at $x = 3$ fm & $y = 0$ fm and the other cell at $x = 7$ fm & $y = 0$ fm. The flows along the y-direction in both cells here are essentially zero due to the symmetry after averaging over many events. For the flow along the x-direction, however, we see that both the profile and magnitude depend significantly on the location even for these central collisions: the flow in the cell closer to the center of the overlap volume develops gradually and then decreases at later times, while the flow in the cell farther away from the center develops very fast and reaches a bigger magnitude. Note that in the AMPT model the centers of the two incoming nuclei are essentially at $x = b/2$ & $y = 0$ fm and $x = -b/2$ & $y = 0$ fm, respectively. As a result, the center of the overlap region of each Au+Au or Pb+Pb event is at $x = 0$ fm & $y = 0$ fm, when event-by-event fluctuations are neglected or when the calculation averages over many events at the same impact parameter.

Fig. 5 shows transverse flows along the x-direction in cells within $-0.5 < y < 0.5$ fm at different locations along the x-axis at various times in central Au+Au collisions at

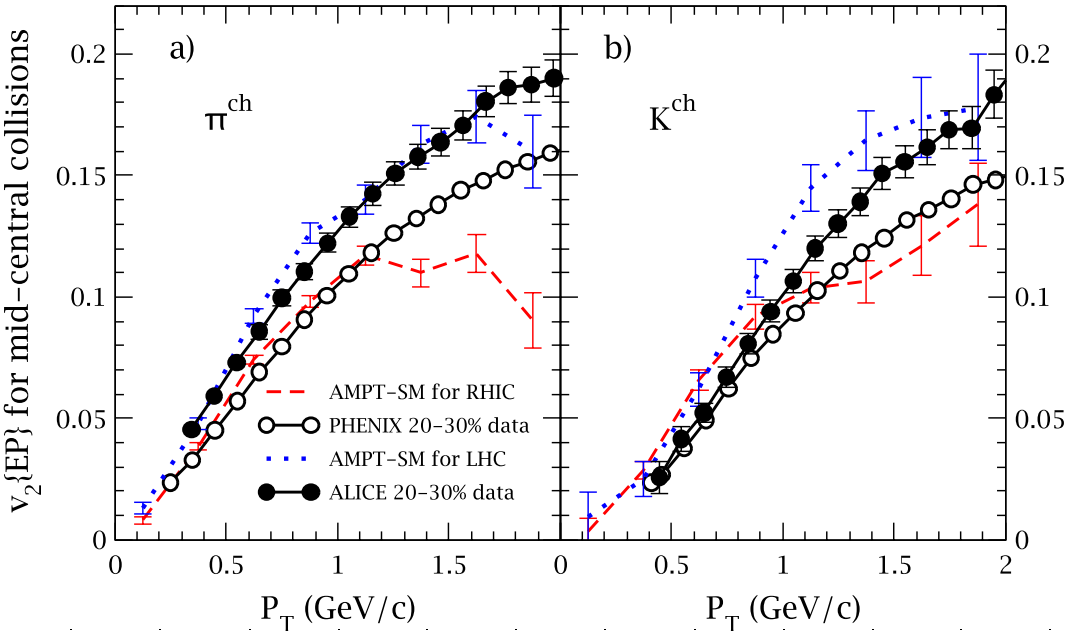

FIG. 3: Elliptic flow $v_2\{\mathrm{EP}\}$ at mid-rapidity in mid-central collisions from AMPT-SM (solid curves) in comparison with experimental data for 20-30% centrality (circles): a) for charged pions, and b) for charged kaons.

RHIC. We see that the flow is initially very small at the early time $t = 0.2$ fm/c and then develops rather fast, while for the inner part of the overlap region ($-4 < x < 4$ fm) the flow decreases appreciably later in the evolution (after $t \sim 8$ fm/c). We also see that in general the flow magnitude is bigger the further away from the overlap center in these central collisions regardless of time t shown in the figure.

IV. SPACE-TIME EVOLUTION OF TEMPERATURE

Partons in a given volume in a heavy ion collision, even after being averaged over many events at the same impact parameter, are in general neither in full thermal equilibrium nor in full chemical equilibrium. Therefore the "temperature" for such a local parton system is only an effective temperature, which value depends on the variable that it is extracted from. In this study we use different variables in the rest frame of a cell, such as the parton mean p_{T}, number density and energy density, to

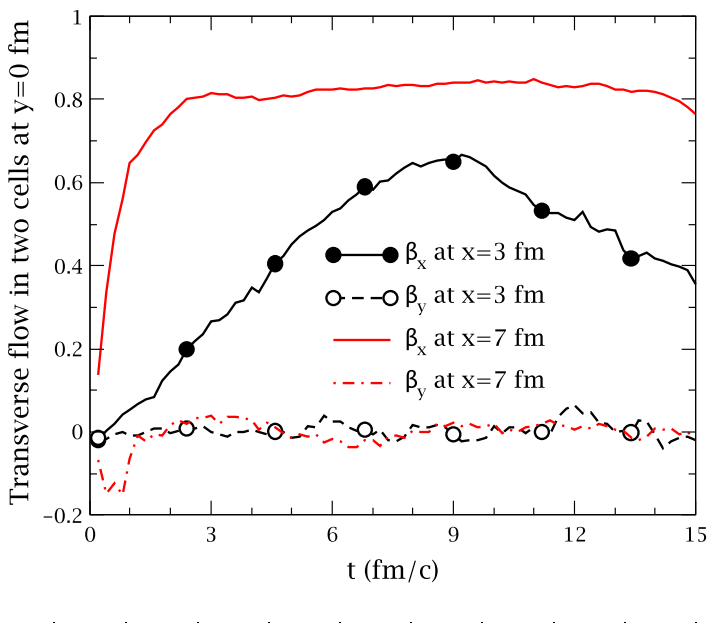

FIG. 4: Transverse flow of partons in the cell at $x = 3$ fm & $y = 0$ fm and in the cell at $x = 7$ fm & $y = 0$ fm as functions of time in central Au+Au collisions at 200 AGeV.

extract the effective temperature of partons in the cell.

To extract the effective temperature from the mean momentum of partons in the rest frame of a cell, we use the relations for a massless parton gas in thermal equilibrium as given by the Boltzmann distribution to get

$$T_{\langle p\rangle} = \frac{\langle p\rangle}{3}, T_{\langle p_{\rm T}\rangle} = \frac{4\,\langle p_{\rm T}\rangle}{3\pi}, T_{\langle p_{\rm T}^2\rangle} = \sqrt{\frac{\langle p_{\rm T}^2\rangle}{8}}. \quad (1)$$

In the above, the bracket represents the mean value of a variable, p represents the magnitude of the parton 3-momentum, and $p_{\rm T}$ represents the parton transverse momentum. Note that quark masses in the parton phase of the AMPT model are current quark masses [10]. Also, the parton phase in the AMPT model does not include the effect of quantum statistics, and the Boltzmann distribution is assumed in the formulae and corresponding curves in this study unless specified otherwise.

We also extract the effective temperature from the number density or energy density of partons in the rest frame of a cell. For this purpose we use the following relations between the densities and temperature T for a massless quark-gluon plasma in full

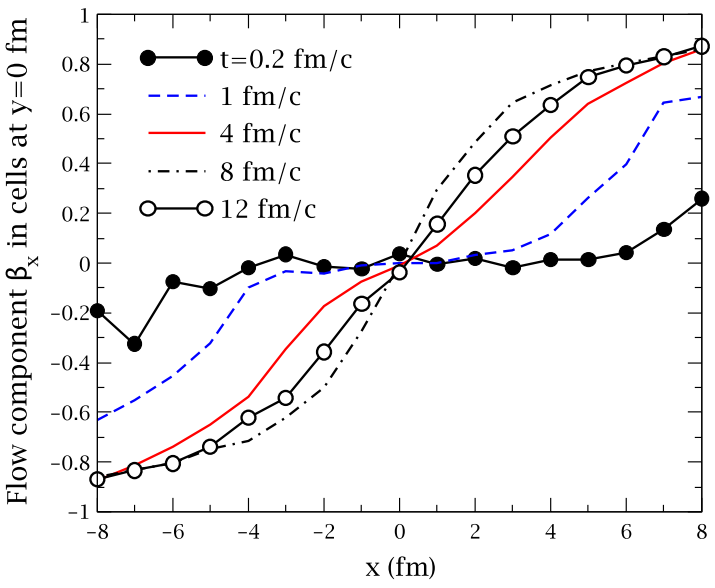

FIG. 5: Flow along the x-direction as functions of x at different times in cells within $-0.5 < y < 0.5$ fm in central Au+Au collisions at 200 AGeV.

chemical and thermal equilibrium as given by the Boltzmann distribution:

$$n = g_{\rm B}\frac{T^3}{\pi^2}, \epsilon_{\rm T} = 3g_{\rm B}\frac{T^4}{4\pi}, \epsilon = 3g_{\rm B}\frac{T^4}{\pi^2}. \tag{2}$$

In the above, n is the parton number density, $\epsilon_{\rm T}$ is the transverse energy density, ϵ is the energy density, $g_{\rm B} \equiv 4(4+3N_f)$ is the total degeneracy factor of QGP when using Boltzmann distributions, and N_f represents the number of relevant quark flavors. We then have the following equations for the corresponding effective temperatures:

$$\begin{aligned} T_n &= 168.\text{MeV}\left(\frac{n\cdot \text{fm}^3}{1+3N_f/4}\right)^{1/3}, \\ T_{\epsilon_{\rm T}} &= 212.\text{MeV}\left(\frac{\epsilon_{\rm T}\cdot \text{fm}^3/\text{GeV}}{1+3N_f/4}\right)^{1/4}, \\ T_{\epsilon} &= 199.\text{MeV}\left(\frac{\epsilon\cdot \text{fm}^3/\text{GeV}}{1+3N_f/4}\right)^{1/4}. \end{aligned} \tag{3}$$

We use the above relations with $N_f = 3$ to extract effective temperatures. Note that using Bose-Einstein and Fermi-Dirac distributions for a massless quark-gluon plasma would lead to $n = (16+9N_f)\zeta(3)T^3/\pi^2$ and $\epsilon = \pi^2(16+10.5N_f)T^4/30$, where $\zeta(3) \simeq$

1.20 is a Riemann zeta function. For $N_f = 3$ they would give $n \simeq 5.24T^3$ and $\epsilon \simeq 15.6T^4$, which are very close to the relations $n \simeq 5.27T^3$ and $\epsilon \simeq 15.8T^4$ when the Boltzmann distribution is used for massless partons as done in Eqs. (2-3).

A. Time evolution of parton densities and mean momentum

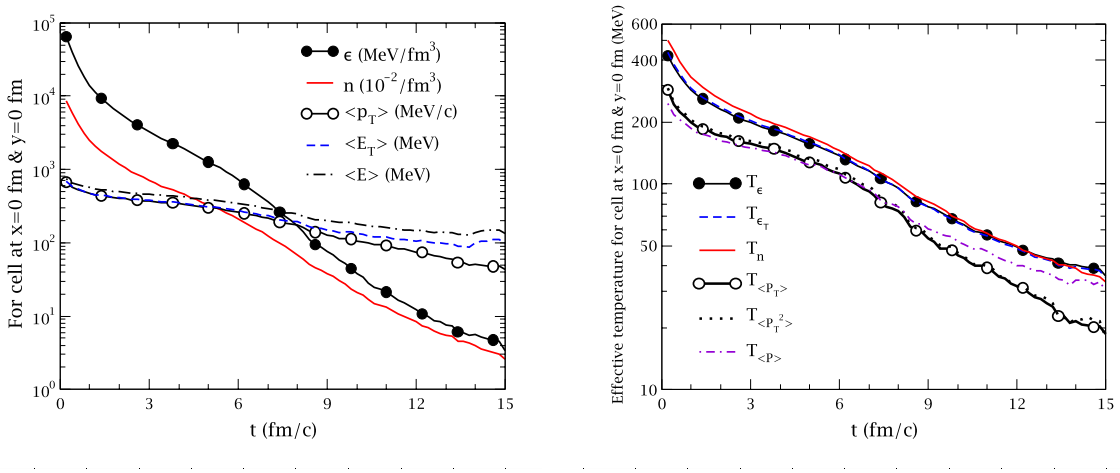

FIG. 6: AMPT-SM results for partons in the rest frame of the center cell in central Au+Au collisions at 200 AGeV. Left panel: time evolutions of the energy density, number density, mean $p_{\rm T}$, mean transverse energy, and mean energy. Right panel: time evolutions of effective temperatures extracted from different variables.

We first examine the parton variables evaluated in the rest frame of the cells, which we shall use to extract the effective temperatures. The left panel of Fig. 6 shows the time evolutions of different variables in the center cell (at $x = 0$ fm & $y = 0$ fm) in central Au+Au collisions at 200 AGeV; they include the parton energy density (filled circles), number density (solid curve), mean $p_{\rm T}$ (open circles), mean transverse energy (dashed curve), and mean energy $\langle E \rangle$ (dot-dashed curve). The parton number density is seen to decrease much faster with time than the parton mean $p_{\rm T}$ or mean energy here. Consequently the parton energy density decreases even faster with time than the parton mean energy, which is expected since $\epsilon \equiv n \langle E \rangle$. We also see that the mean $p_{\rm T}$ and mean transverse energy are essentially the same at early times, and then they

separate at late times when parton mass (especially the strange quark mass) plays a bigger role as the mean $p_{\rm T}$ becomes smaller. Furthermore, the amount by which the parton mean energy is above the mean transverse energy reflects the contribution from the squared longitudinal momentum $p_{\rm z}^2$ of partons under consideration (i.e. within $|\eta| < 1/2$).

B. Time evolution of effective temperatures

The right panel of Fig. 6 shows time evolutions of effective temperatures extracted from different variables via Eqs. (1-3) for the center cell in central Au+Au collisions at 200 AGeV. Here we see that the effective temperatures extracted from the parton energy density (filled circles), number density (solid curve), and transverse energy density (dashed curve) are all significantly higher than those extracted from the shown mean momentum variables, i.e., those extracted from the parton mean $p_{\rm T}$ (open circles), mean $p_{\rm T}^2$ (dotted curve), and mean 3-momentum (dot-dashed curve). We also see that effective temperature T_ϵ extracted from the parton energy density is very close to $T_{\epsilon_{\rm T}}$ that is extracted from the parton transverse energy density throughout the time evolution. While the effective temperature $T_{\langle p_{\rm T}\rangle}$ extracted from the parton mean $p_{\rm T}$ is very close to $T_{\langle p_{\rm T}^2\rangle}$ that is extracted from the parton mean $p_{\rm T}^2$, it is higher than $T_{\langle p\rangle}$ (extracted from the parton mean 3-momentum) at early times and then lower than $T_{\langle p\rangle}$ at late times. This suggests that the mean squared longitudinal momentum $p_{\rm z}^2$ is lower than the mean squared momentum along a transverse direction at early times but higher than that at later times; this is consistent with an earlier study on the pressure anisotropy in the AMPT model [29], where the ratio of the longitudinal pressure over the transverse pressure starts initially below one but then quickly exceeds one after a time of several fm/c. Recently pressure anisotropy has also been considered within the hydrodynamic framework [30–32].

From the right panel of Fig. 6, we also observe that T_ϵ is mostly between $T_{\langle p_{\rm T}\rangle}$ and T_n, the effective temperatures extracted from the parton while being close to T_n. This can be understood in the following. Relation $\epsilon_{\rm T} = n\,\langle E_{\rm T}\rangle$ gives

$$T_{\epsilon_{\rm T}}^4 = T_n^3\; T_{\langle E_{\rm T}\rangle}. \tag{4}$$

Since $T_{\epsilon_{\rm T}} \simeq T_\epsilon$ as shown in the right panel of Fig. 6 and at high densities $\langle E_{\rm T}\rangle \simeq \langle p_{\rm T}\rangle$ as shown in the left panel of Fig. 6, we can write

$$T_\epsilon^4 \simeq T_n^3\, T_{\langle p_{\rm T}\rangle}. \tag{5}$$

We find that the above relation for T_ϵ is a good approximation at moderately high densities: for all cells within $|\eta| < 1/2$ in all four collisions systems that we considered, the actual T_ϵ value is found to be always within 6% of the value as given by Eq. (5) if $T_\epsilon > 100$ MeV in the cell.

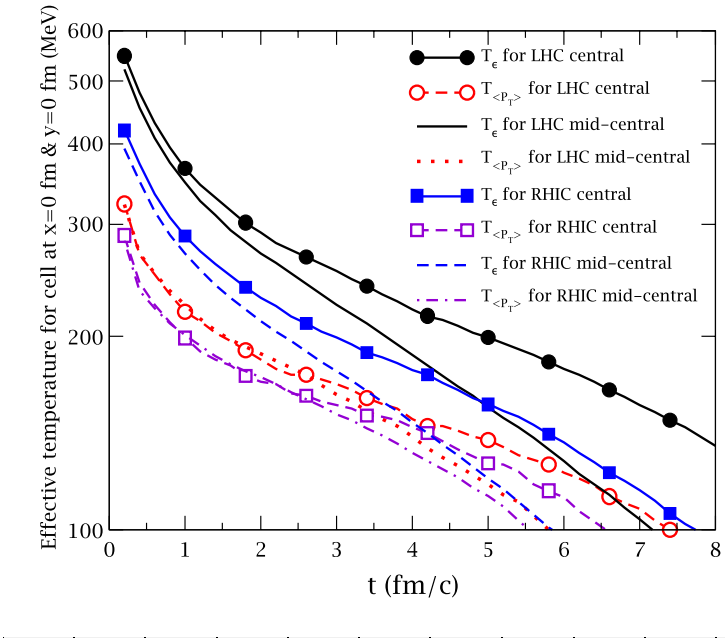
Effective temperature for cell at x=0 fm & y=0 fm (MeV)
t (fm/c)
T_ε for LHC central
T_<P_T> for LHC central
T_ε for LHC mid-central
T_<P_T> for LHC mid-central
T_ε for RHIC central
T_<P_T> for RHIC central
T_ε for RHIC mid-central
T_<P_T> for RHIC mid-central

FIG. 7: AMPT-SM results on effective temperatures as functions of time for the center cell in central and mid-central Pb+Pb collisions at 2760 AGeV and Au+Au collisions at 200 AGeV.

Fig. 7 shows the time evolutions of T_ϵ and $T_{\langle p_{\rm T}\rangle}$ in the center cell in these different collisions, and we see $T_\epsilon > T_{\langle p_{\rm T}\rangle}$ in each case. It is also seen that the initial temperature T_ϵ (and $T_{\langle p_{\rm T}\rangle}$) in mid-central collisions is similar to that in central collisions at the same energy, but the temperature in mid-central collisions decreases faster with time. On the other hand, the initial temperature T_ϵ (and $T_{\langle p_{\rm T}\rangle}$) in LHC collisions is higher than that in RHIC collisions at the same centrality, but the shape of the temperature evolution

with time looks similar at these two energies.

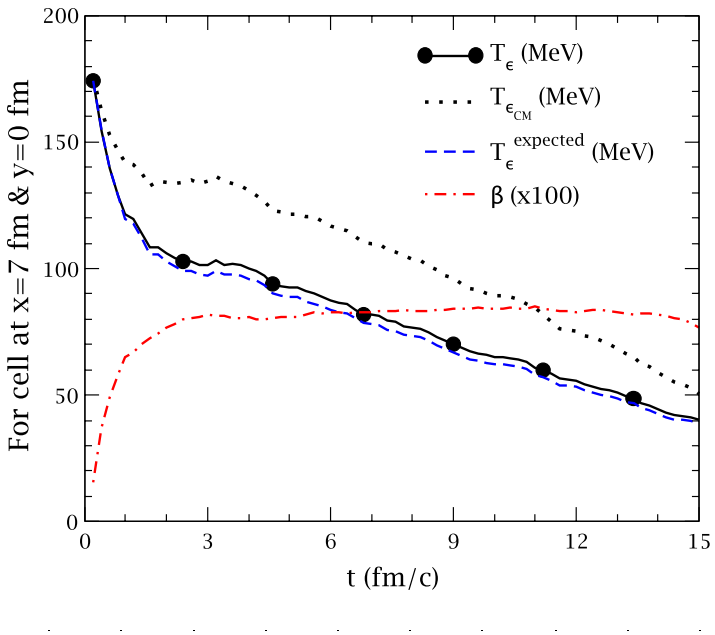

FIG. 8: AMPT-SM results on effective temperatures as functions of time for the cell at $x = 7$ fm & $y = 0$ fm in central Au+Au collisions at 200 AGeV; the dot-dashed curve represents the flow magnitude (multiplied by 100) in the cell.

We have also checked the relation between T_ϵ extracted from the parton energy density in the rest frame of the cell and $T_{\epsilon_{\rm CM}}$, which is the "apparent" temperature if one simply converts the energy density of the cell in the center-of-mass (CM) frame into temperature using Eq. (3). Fig. 8 shows the time evolutions of T_ϵ (filled circles) and $T_{\epsilon_{\rm CM}}$ (dotted curve) in the cell at $x = 7$ fm & $y = 0$ fm in central Au+Au collisions at 200 AGeV, where the "apparent" temperature $T_{\epsilon_{\rm CM}}$ is much higher than T_ϵ after 1 fm/c. For a volume cell that can be described by energy density ϵ and pressure P, the energy density ϵ in its rest frame is related to the energy density $\epsilon_{\rm CM}$ in the CM frame by

$$\epsilon_{\rm CM} = \gamma^2(\epsilon + P) - P, \tag{6}$$

where γ is the Lorentz factor for the moving cell in the CM frame. Using $P = \epsilon/3$ for

a massless parton gas, we get

$$\epsilon = \epsilon_{\rm CM}\left(\frac{3}{4\gamma^2-1}\right),$$
$$T_\epsilon^{\rm expected} = T_{\epsilon_{\rm CM}}\left(\frac{1-\beta^2}{1+\beta^2/3}\right)^{1/4}, \quad (7)$$

where β is the magnitude of the flow of the cell in the CM frame. Using the flow magnitude β shown as the dot-dashed curve in Fig. 8, Eq. (7) gives $T_\epsilon^{\rm expected}$ (the expected value of T_ϵ) as the dashed curve, which is very close to the actual T_ϵ calculated directly from the energy density in the rest frame of the cell. The small difference between T_ϵ and $T_\epsilon^{\rm expected}$ may come from the fact that partons are not massless and that pressures along different axes are not fully isotropicalized during the evolution [29, 33].

C. Spatial dependence of effective temperatures

We now look at how the effective temperatures depend on location in the overlap volume. Fig. 9 shows how T_ϵ and $T_{\langle p_{\rm T}\rangle}$ change with location along the impact parameter axis at different times: $t = 0.2, 2.0$ and 5.0 fm/c. In both central Pb+Pb collisions at 2760 AGeV and mid-central Au+Au collisions at 200 AGeV, we see that the initial effective temperatures $T_{\langle p_{\rm T}\rangle}$ at $t = 0.2$ fm/c change little over most of the overlap volume. We also see that $T_\epsilon > T_{\langle p_{\rm T}\rangle}$ over the inner part of the overlap volume, e.g., within $|x| < 6$ fm for central Pb+Pb collisions at 2760 AGeV and within $|x| < 3$ fm for mid-central Au+Au collisions at 200 AGeV at $t = 0.2$ fm/c. Note that, in order to limit the statistical fluctuations, volume cells that have less than 20 partons after summing over simulated events are not shown in Figs. 9-10.

The spatial dependences of effective temperatures T_ϵ and $T_{\langle p_{\rm T}\rangle}$ in the four different collisions are shown in Fig. 10a for $t = 0.2$ fm/c and in Fig. 10b for $t = 5.0$ fm/c. From Fig. 10a we find that the initial effective temperatures $T_{\langle p_{\rm T}\rangle}$ for central and mid-central Pb+Pb collisions at 2760 AGeV are almost the same in the overlap volume except that the spatial width is smaller for mid-central collisions. In contrast, the initial effective temperatures T_ϵ for central LHC collisions are higher and much wider

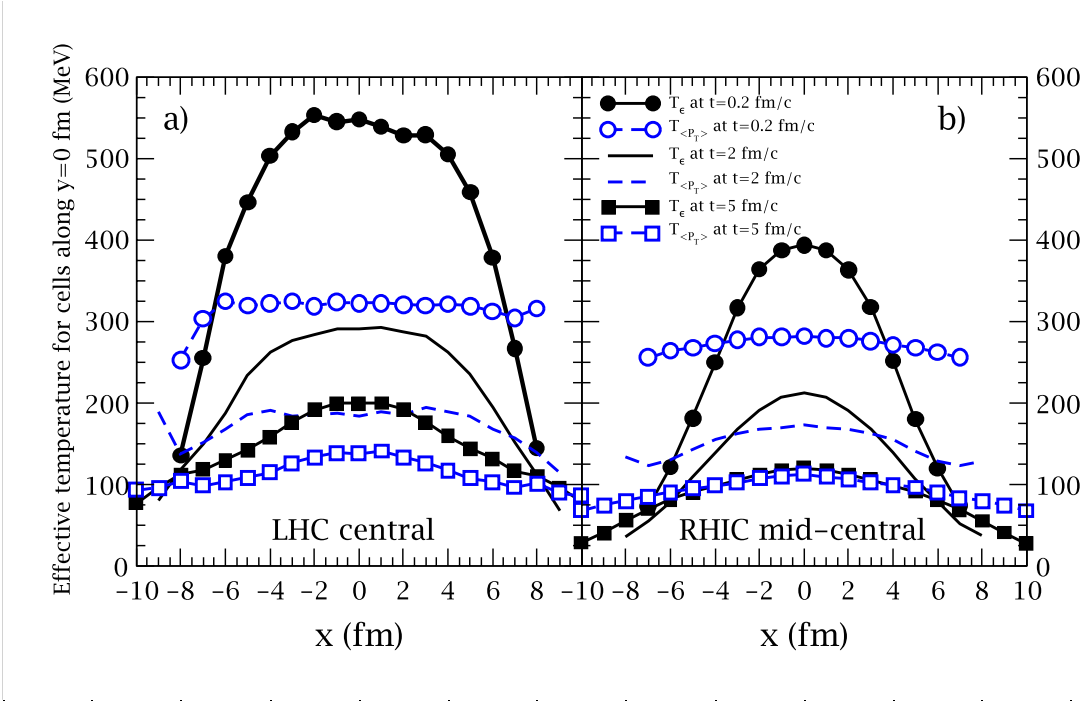

FIG. 9: AMPT-SM results on effective temperatures in cells along the impact parameter at $t = 0.2, 2.0$ and 5.0 fm/c: a) for central Pb+Pb collisions at 2760 AGeV, and b) for mid-central Au+Au collisions at 200 AGeV.

in spatial width than those in mid-central LHC collisions. These features are also seen in results at the RHIC energy. Furthermore, although the initial temperatures T_ϵ in mid-central Pb+Pb collisions at 2760 AGeV are higher than those in central Au+Au collisions at 200 AGeV in the inner part of the overlap volume, the width of T_ϵ along the impact parameter axis is smaller. From Fig. 10b one sees that the initial effective temperature T_ϵ for central LHC collisions are overall significantly higher than the other collisions systems. In addition, temperatures T_ϵ and $T_{\langle p_{\rm T}\rangle}$ at $t = 5.0$ fm/c are mostly similar for mid-central Pb+Pb collisions at 2760 AGeV and central Au+Au collisions at 200 AGeV, suggesting that the lifetime of the quark-gluon plasma is similar in these two collision systems.

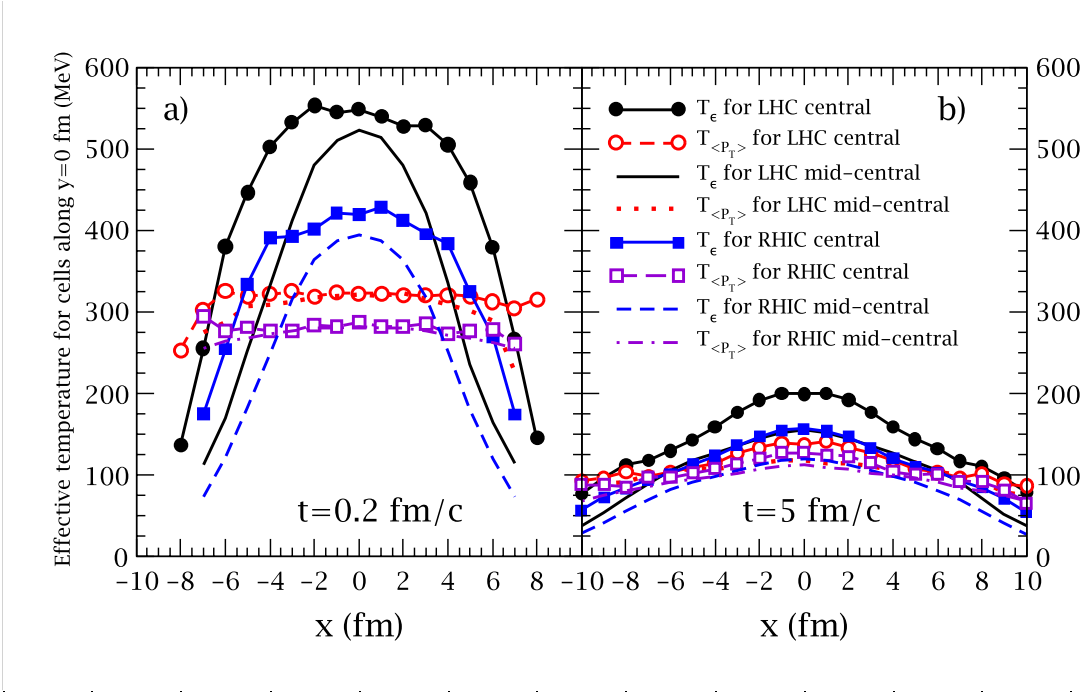

FIG. 10: AMPT-SM results on effective temperatures in cells along the impact parameter for different collisions: a) at $t = 0.2$ fm/c, and b) at $t = 5.0$ fm/c.

D. Over-population of partons

We have already seen from Figs. 9-10 that $T_\epsilon > T_{\langle p_T \rangle}$ over the inner part of the overlap volume in these high energy heavy ion collisions, and this is essentially due to $T_n > T_{\langle p_T \rangle}$ according to Eq. (5). This reflects the fact that the parton system in a subvolume of the overlap region in such a collision, even after being averaged over many events at the same impact parameter, is not in full chemical equilibrium as defined for an ideal quark-gluon plasma. The relation $T_n > T_{\langle p_T \rangle}$ means that for the parton number density we have $n > n(T_{\langle p_T \rangle})$, where $n(T_{\langle p_T \rangle})$ is the parton number density expected for a quark-gluon plasma in full chemical equilibrium at temperature $T_{\langle p_T \rangle}$. For example, $T_\epsilon \sim 1.7\ T_{\langle p_T \rangle}$ in Figs. 9a for $x = 0$ fm at $t = 0.2$ fm/c in central LHC collisions means that, according to Eq. (3) and the approximation of Eq. (5), $n \sim 1.7^4\ n(T_{\langle p_T \rangle}) \simeq 8.4\ n(T_{\langle p_T \rangle})$ for that center cell at that time. Later at $t = 5.0$ fm/c, we see in Figs. 9b that $T_\epsilon \sim 1.44\ T_{\langle p_T \rangle}$, which gives $n \sim 4.3\ n(T_{\langle p_T \rangle})$ at that time. Therefore one may say that the parton system in that subvolume is over-populated, in

that the parton density is too high compared to that expected for an ideal QGP that has the same parton mean transverse momentum.

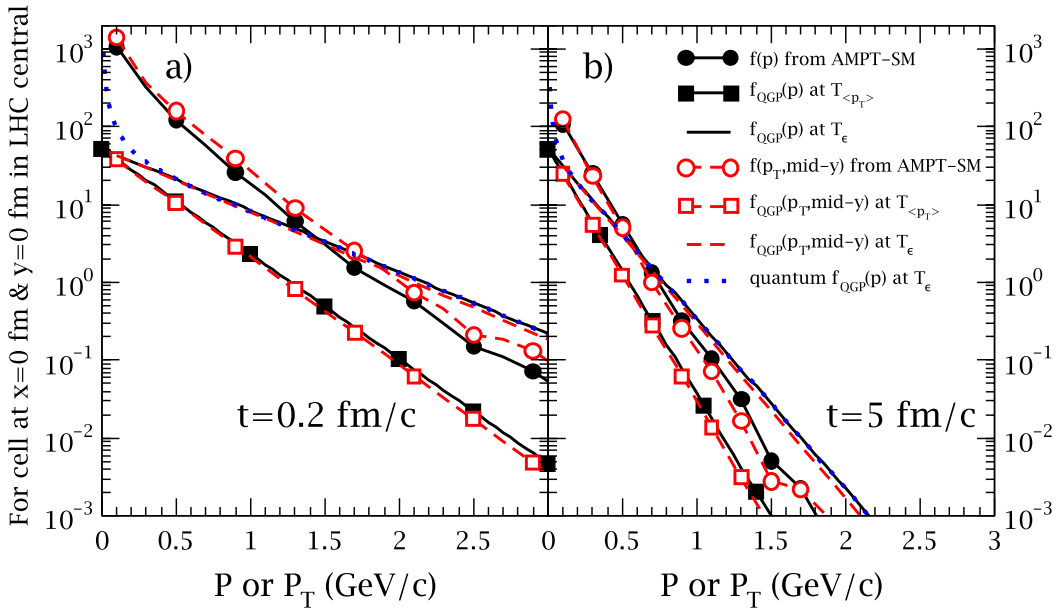

FIG. 11: Phase space distribution of partons in the center cell in central Pb+Pb collisions at 2760 AGeV versus momentum p (solid curves) or versus $p_{\rm T}$ at mid-rapidity (dashed curves) a) at $t = 0.2$ fm/c, and b) at $t = 5.0$ fm/c. Circles represent results from the AMPT-SM model, curves with squares represent an ideal QGP at temperature $T_{\langle p_{\rm T}\rangle}$, solid and dashed curves without symbols represent an ideal QGP at temperature T_ϵ, and dotted curves represent an ideal QGP at temperature T_ϵ with quantum statistics.

To further illustrate this, we calculate the phase space density of partons. In terms of the magnitude of parton 3-momentum in the rest frame of a cell, we have

$$f(p) \equiv (2\pi)^3 \frac{dN}{d^3x d^3p} = 2\pi \frac{dN/d^3x}{p^2 dp}. \tag{8}$$

We also calculate the phase space density in terms of parton $p_{\rm T}$ at a given rapidity y in the rest frame of a cell, where one can write

$$f(p_{\rm T}, y) = 4\pi^2 \frac{dN/d^3x}{p_{\rm T} dp_{\rm T} dp_{\rm z}}. \tag{9}$$

We choose mid-rapidity partons, i.e., partons within $|y| < 1/2$ in the rest frame of the cell. By approximating the parton system as massless, which is a reasonable approximation when the temperature is high (see left panel of Fig. 6), we can obtain

$$f(p_{\rm T}, {\rm mid-y}) \simeq 4\pi^2 \frac{dN/d^3x}{p_{\rm T} dp_{\rm T} \Delta p_{\rm z}} \simeq \frac{4\pi^2}{2\sinh(1/2)} \frac{dN/d^3x}{p_{\rm T}^2 dp_{\rm T}}, \tag{10}$$

where $\Delta p_{\rm z}$ represents the longitudinal momentum range under consideration. For comparison, the expected phase space distribution for an ideal QGP at temperature T is given by

$$f_{\rm QGP}(p) = g_{\rm B} e^{-E/T} \simeq g_{\rm B} e^{-p/T}, f_{\rm QGP}(p_{\rm T}, y) = g_{\rm B} e^{-m_{\rm T}\cosh(y)/T}, \tag{11}$$

when the Boltzmann distribution is used for partons that are assumed to be massless. We then make the following approximation for mid-rapidity:

$$f_{\rm QGP}(p_{\rm T}, {\rm mid-y}) \simeq g_{\rm B} e^{-p_{\rm T}\cosh(1/4)/T}. \tag{12}$$

The AMPT-SM results for the center cell at two different times in central Pb+Pb collisions at 2760 AGeV are shown in Fig. 11, in comparison with the expected phase space distributions for an ideal QGP at the corresponding temperature T_ϵ (548 MeV at $t = 0.2$ fm/c and 199 MeV at $t = 5$ fm/c) or $T_{\langle p_{\rm T}\rangle}$ (322 MeV at $t = 0.2$ fm/c and 138 MeV at $t = 5$ fm/c). We first see that the AMPT-SM results (curves with circles) and the expected curves for an ideal QGP at temperature $T_{\langle p_{\rm T}\rangle}$ (curves with squares) at a given time have a similar overall slope. This reflects the fact that the effective temperature $T_{\langle p_{\rm T}\rangle}$ is only determined by the parton mean $p_{\rm T}$ in the cell; it also indicates that the $p_{\rm T}$ distribution of partons in the subvolume here is not too far from a thermal distribution. In the meantime, the AMPT-SM curves are much higher in magnitude than the ideal QGP curves at temperature $T_{\langle p_{\rm T}\rangle}$, suggesting that the parton matter is over-populated by a large factor. When compared with the expected distributions for an ideal QGP at temperature T_ϵ (solid and dashed curves without symbols), partons in the AMPT-SM results are still over-populated below a given value of $p_{\rm T}$ or p. This value is smaller at a later time as shown in Fig. 11: partons in that center cell are seen to be over-populated below $p_{\rm T} \simeq 1.4$ GeV/c at $t = 0.2$ fm/c but below $p_{\rm T} \simeq 0.6$ GeV/c at $t = 5$ fm/c, when compared with an ideal QGP at temperature T_ϵ.

From Fig. 11 we see that the phase space distributions in momentum p or $p_{\rm T}$ are quite close to each other. At zero-momentum, both $f_{\rm QGP}(p)$ and $f_{\rm QGP}(p_{\rm T}, {\rm mid-y})$ approach the value $g_{\rm B} = 52$ (the degeneracy factor of QGP for $N_f = 3$) for an ideal QGP with Boltzmann statistics. Considering Fermi-Dirac statistics, the phase space densities of quarks and anti-quarks are bound to be below one for each degree of freedom due to the Pauli exclusion principle, therefore the phase space density contributed from quarks and anti-quarks must be below $12N_f = 36$ (their total degeneracy factor for $N_f = 3$) regardless of temperature. Therefore the high phase space densities above this value shown in Fig. 11 cannot be explained by a full population of the phase space by quarks and antiquarks. It cannot be explained by the Bose-Einstein distribution of gluons in an ideal QGP either. Dotted curves in Fig. 11 represent the expected quantum phase space distributions at temperature T_ϵ when Bose-Einstein and Fermi-Dirac distributions are used for a massless quark-gluon plasma:

$$f_{\rm QGP}^{quantum}(p) = \frac{16}{e^{p/T} - 1} + \frac{12N_f}{e^{p/T} + 1}. \tag{13}$$

For an ideal QGP, we see that the expected quantum phase space densities are very close to the expected Boltzmann densities except at very low $p_{\rm T}$, and the AMPT-SM results are still much higher than the quantum phase space densities except at very low $p_{\rm T}$. Since there is no bound for the gluon phase space densities due to quantum statistics, one may argue that the high density regions as shown in Fig. 11 indicate that at least gluons are over-populated there. This may be analogous to the glasma produced from the color-glass-condensate [2, 34].

Therefore, when the parton system in a volume cell satisfies $n > n(T_{\langle p_{\rm T}\rangle})$, we consider partons in that cell as being over-populated relative to an ideal QGP at temperature $T_{\langle p_{\rm T}\rangle}$. So we use the AMPT-SM results to investigate regions within $|\eta| < 1/2$ that have over-populated partons. We first define a "critical" temperature T_c above which a dense matter can be considered as being well inside the QGP phase, then a cell that satisfies the condition $T_\epsilon > T_c$ is called a QGP cell, and a QGP cell that also satisfies the condition $T_\epsilon > T_{\langle p_{\rm T}\rangle}$ is called a over-populated cell. In this study we take $T_c = 150$ MeV, which corresponds to a "critical" energy density $\epsilon_c = 1.05$ GeV/fm^3 for $N_f = 3$ as given by Eq. (3).

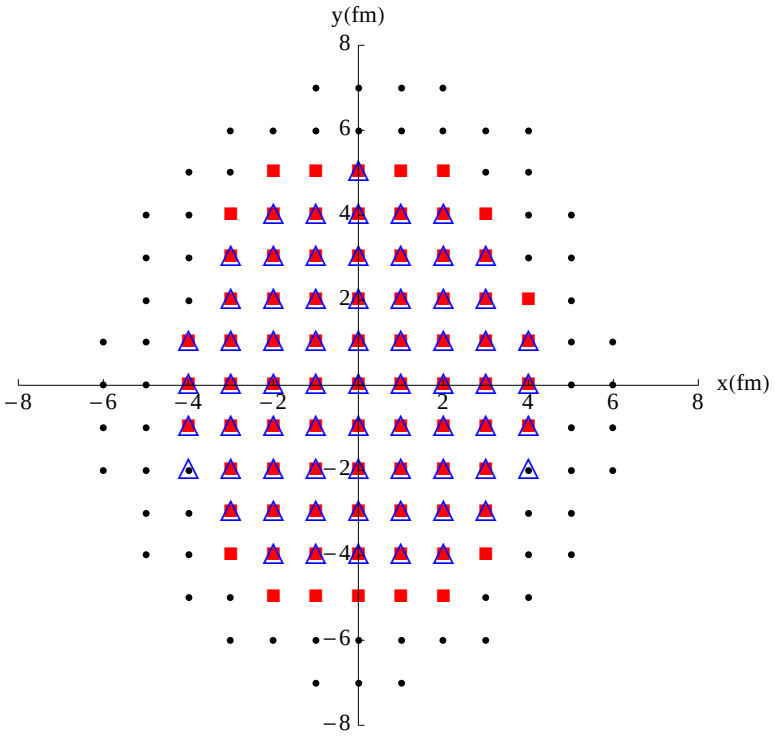

FIG. 12: For partons within $|\eta| < 1/2$ in mid-central Pb+Pb collisions at 2760 AGeV, filled circles represent the center locations in the transverse plane for QGP cells at $t = 0.2$ fm/c, filled squares represent over-populated QGP cells at $t = 0.2$ fm/c, and open triangles represent over-populated QGP cells at $t = 3.0$ fm/c.

Fig. 12 shows the transverse locations of QGP cells (i.e. with $T_\epsilon > T_c$) and over-populated cells (i.e. with $T_\epsilon > T_c$ and $T_\epsilon > T_{\langle p_{\rm T}\rangle}$) in mid-central Pb+Pb collisions at 2760 AGeV. We can see that at $t = 0.2$ fm/c the initial extension of QGP cells (filled circles) along the y-axis is bigger than that along the x-axis due to the spatial asymmetry in mid-central collisions. More that half of these QGP cells are over-populated at this early time, as indicated by filled squares, and they are located in the inner part of the overlap volume. Later at $t = 3.0$ fm/c, QGP cells that are over-populated (open triangles) still occupy an area in the transverse plane almost as large as that at $t = 0.2$ fm/c (filled squares), while the shape of overpopulated cells in the transverse plane at $t = 3.0$ fm/c has a smaller spatial asymmetry than that at $t = 0.2$ fm/c.

In Fig. 13 we show the transverse areas of QGP cells and the transverse areas of

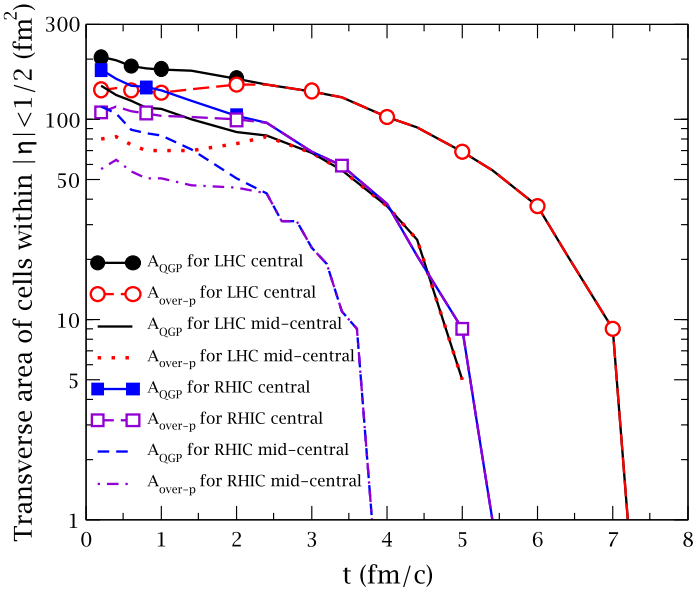

FIG. 13: Transverse areas of QGP cells ($A_{\rm QGP}$) and transverse areas of QGP cells that are over-populated ($A_{\rm over-p}$) as functions of time for different collisions.

over-populated QGP cells as functions of time in different collisions. Note that each cell here covers $|\eta| < 1/2$ along the beam direction. For all four collisions systems, we see that initially a significant fraction, roughly from 50% to 70%, of the QGP cells are over-populated with partons. This fraction is higher for central collisions than mid-central collision at the same energy and also higher for the LHC energy than the RHIC energy at the same centrality. After 2-3 fm/c, however, all QGP cells are over-populated. Although the transverse area of QGP cells decreases monotonously over time, the transverse area of over-populated cells does not change much and may even slightly increase over the first several fm/c of time. One also sees that the areas in central RHIC collisions are mostly bigger than the corresponding areas in mid-central LHC collisions even though the peak temperature in central RHIC collisions is lower (as shown in Fig. 10a), while the QGP phases in the two collision systems show a similar lifetime.

V. DISCUSSIONS

The string melting version [10, 15] of the AMPT model only has quarks and anti-quarks in the parton phase. This is not to be considered as physical though, since one expects gluons to dominate the initial stage of ultra-relativistic heavy ion collisions and gluons will be produced from quark and anti-quark interactions. The lack of gluons in the AMPT-SM model results from our inability to consistently address gluon and quark productions from a strong color field [10]. However, the AMPT-SM model enables us to include the energy from all the excited strings in the overlap volume into the parton transport. For studies that depend more on the effect of partonic scatterings instead of the composition of the partonic matter, such as studies of the elliptic flow [15] and the pion interferometry [35], it is suitable to use the AMPT-SM model. Since this study addresses the time evolution of parton flow, mean momentum or energy, number density, and energy density, its results depend mostly on the effect of partonic scatterings but not on the composition of the partonic matter. We then inferred from the effective temperatures T_ϵ and $T_{\langle p_{\rm T}\rangle}$, which are extracted respectively from the parton energy density and mean $p_{\rm T}$, that the high density matter in the inner region of the overlap volume in these collisions are over-populated with partons (at least over-populated with gluons), even though the AMPT-SM model has no gluons in the parton phase.

The parton cascade in the AMPT model only include elastic parton scatterings. Including inelastic parton scatterings in the parton cascade [9, 33] would change the space-time evolution of the dense parton matter and thus affect the transverse flow and effective temperatures. Unfortunately we do not yet have a multi-phase transport model that includes inelastic parton reactions. However, since the initial condition from the AMPT-SM model would not be affected by the subsequent parton scatterings, the results in this study at $t = 0.2$ fm/c would remain the same. Therefore our qualitative conclusions about the mismatch among different effective temperatures and about the over-population in the inner part of the overlap volume would not change; while the time evolutions of the temperature mismatch and over-populated areas would be affected by inelastic parton scatterings.

The space-time evolution data obtained from this study may serve as a bulk matter background for studies such as jet propagation and interactions with the partonic matter within the JET Collaboration [22, 36] and beyond. The effective temperatures extracted from the parton phase in the AMPT-SM model also provide a link to hydrodynamic models. Currently one may argue that T_ϵ is a reasonable choice for the effective temperature of the parton system, because it takes into account both the density and the mean momentum of the local parton system. Also, the essential variable in the hydrodynamic approach is the local energy-momentum tensor, and using T_ϵ ensures that the local energy distributions remain the same when the transport approach is linked to the hydrodynamic approach. However, since the effective temperatures depend on the variables from which they are extracted, further studies will be necessary to address the uncertainty associated with this dependence. As we have seen, the mismatch between T_ϵ and $T_{\langle p_{\rm T}\rangle}$ could be attributed to an over-population of partons in the dense matter, thus the uncertainty about the effective temperatures reflects the uncertainty in the initial conditions for ultra-relativistic heavy ion collisions.

VI. CONCLUSIONS

We have studied the space-time evolution of the parton phase created in heavy ion collisions at RHIC and LHC energies using the AMPT model with string melting, which converts excited hadronic strings in the overlap volume into partons. Several key parameters in the model have been tuned to reproduce the low-$p_{\rm T}$ data on the pion and kaon yields, $p_{\rm T}$ spectra and elliptic flows. This way the space-time evolution from the model is more reliable, and it may serve as a bulk matter background for studies such as jet propagation and interactions with the partonic matter.

This study focuses on the effective temperatures in different volume cells within mid-spacetime-rapidity $|\eta| < 1/2$. Many events at the same impact parameter are averaged over in order to have enough statistics for the analysis of each volume cell, and as a result this study does not address the effect of event-by-event fluctuations. Since the parton system in a subvolume is in general neither in full thermal equilibrium nor in full chemical equilibrium, the value of the effective temperature depends, sometimes

strongly, on the variable that it is extracted from. We have extracted effective temperatures from several different variables that are evaluated in the rest frame of each cell. We find that temperature T_ϵ extracted from the parton energy density is often very different from $T_{\langle p_{\rm T}\rangle}$ extracted from the parton mean $p_{\rm T}$, and it is mostly between $T_{\langle p_{\rm T}\rangle}$ and T_n extracted from the parton number density while being closer to T_n. For these collisions we also find that $T_\epsilon > T_{\langle p_{\rm T}\rangle}$ over the inner part of the overlap volume, which indicates that partons (at least gluons) are over-populated there. This is also checked by the examination of parton phase space densities. Our results show that at mid-spacetime-rapidity initially about half or more QGP cells, defined as cells that are above a critical energy density of 1 GeV/fm^3, are over-populated. The initial fraction of over-populated cells is found to be bigger at higher energies and in more central collisions. We also find that all QGP cells are over-populated after a couple of fm/c, and the total transverse area of over-populated cells does not change much during the first few fm/c.

VII. ACKNOWLEDGMENTS

The author would like to thank B. Betz for valuable discussions and express special thanks to M. Gyulassy for motivating this study. As an external associate, the author thanks the JET Collaboration for help. The author also thanks Dr. X.-N. Wang for updating the JET Collaboration wiki page with the link to the data files from this study.

[1] B. Alver and G. Roland, Phys. Rev. C **81**, 054905 (2010) [Erratum-ibid. C **82**, 039903 (2010)].

[2] J. -P. Blaizot, F. Gelis, J. -F. Liao, L. McLerran and R. Venugopalan, Nucl. Phys. A **873**, 68 (2012).

[3] B. Betz and M. Gyulassy, Phys. Rev. C **86**, 024903 (2012).

[4] S. Chatrchyan *et al.* [CMS Collaboration], Phys. Lett. B **718**, 795 (2013).

[5] P. Huovinen, P. F. Kolb, U. W. Heinz, P. V. Ruuskanen and S. A. Voloshin, Phys. Lett. B **503**, 58 (2001).

[6] B. Betz, J. Noronha, G. Torrieri, M. Gyulassy, I. Mishustin and D. H. Rischke, Phys. Rev. C **79**, 034902 (2009).

[7] B. Schenke, S. Jeon and C. Gale, Phys. Rev. Lett. **106**, 042301 (2011).

[8] P. Bozek, Phys. Rev. C **85** (2012) 014911.

[9] Z. Xu and C. Greiner, Phys. Rev. C **71**, 064901 (2005).

[10] Z. -W. Lin, C. M. Ko, B. -A. Li, B. Zhang and S. Pal, Phys. Rev. C **72**, 064901 (2005).

[11] W. Cassing and E. L. Bratkovskaya, Nucl. Phys. A **831**, 215 (2009).

[12] H. Petersen, J. Steinheimer, G. Burau, M. Bleicher and H. Stocker, Phys. Rev. C **78**, 044901 (2008).

[13] K. Werner, I. .Karpenko, T. Pierog, M. Bleicher and K. Mikhailov, Phys. Rev. C **82**, 044904 (2010).

[14] H. Song, S. A. Bass, U. Heinz, T. Hirano and C. Shen, Phys. Rev. Lett. **106**, 192301 (2011) [Erratum-ibid. **109**, 139904 (2012)].

[15] Z. -W. Lin and C. M. Ko, Phys. Rev. C **65**, 034904 (2002).

[16] B. Zhang, C. M. Ko, B. -A. Li and Z. -W. Lin, Phys. Rev. C **61**, 067901 (2000).

[17] Z. -W. Lin, S. Pal, C. M. Ko, B. -A. Li and B. Zhang, Phys. Rev. C **64**, 011902 (2001).

[18] T. Sjostrand, Comput. Phys. Commun. **82**, 74 (1994).

[19] J. Xu and C. M. Ko, Phys. Rev. C **83**, 034904 (2011).

[20] Grid data files of the space-time evolution of the parton matter from this study has been posted at http://personal.ecu.edu/linz/ampt/evolutiondata/; the link has also been posted at the JET Collaboration wiki page https://sites.google.com/a/lbl.gov/jetwiki/code-packages/hydro-evolution/.

[21] B. Betz and M. Gyulassy, arXiv:1305.6458 [nucl-th].

[22] K. M. Burke, A. Buzzatti, N. Chang, C. Gale, M. Gyulassy, U. Heinz, S. Jeon and A. Majumder *et al.*, arXiv:1312.5003 [nucl-th].

[23] B. Abelev *et al.* [ALICE Collaboration], Phys. Rev. C **88**, 044910 (2013).

[24] A. Adare *et al.* [PHENIX Collaboration], Phys. Rev. C **87**, 034911 (2013).

[25] B. Abelev *et al.* [ALICE Collaboration], Phys. Rev. C **88**, 044909 (2013).

[26] S. S. Adler *et al.* [PHENIX Collaboration], Phys. Rev. C **69**, 034909 (2004).

[27] Y. Gu [PHENIX Collaboration], Nucl. Phys. A **904-905**, 353c (2013).

[28] G. Aad *et al.* [ATLAS Collaboration], Phys. Rev. C **86**, 014907 (2012).

[29] B. Zhang, L. -W. Chen and C. M. Ko, J. Phys. G **35**, 065103 (2008).

[30] W. Florkowski and R. Ryblewski, Phys. Rev. C **83**, 034907 (2011).

[31] M. Martinez and M. Strickland, Nucl. Phys. A **848**, 183 (2010).

[32] D. Bazow, U. W. Heinz and M. Strickland, arXiv:1311.6720 [nucl-th].

[33] Z. Xu and C. Greiner, Phys. Rev. C **76**, 024911 (2007).

[34] T. Lappi and L. McLerran, Nucl. Phys. A **772**, 200 (2006).

[35] Z. W. Lin, C. M. Ko and S. Pal, Phys. Rev. Lett. **89**, 152301 (2002).

[36] Topical Collaboration on Jet and Electromagnetic Tomography of Extreme Phases of Matter in Heavy-ion Collisions, webpage at http://jet.lbl.gov